BEHAVIOUR OF PRESTRESSED HOLLOW-CORE CONCRETE SLAB UNDER FIRE – EXPERIMENTAL STUDY

Neno Torić, Vladimir Divić, Ivica Boko

Original scientific paper

The paper presents an experimental study of behaviour of a prestressed hollow-core slab exposed to ISO fire curve. Dimensions of the slab are $1,2 \times 8,0$ m. The study includes measurements of temperature gradient inside the section of the slab, voids, and upper surface of the slab. Time dependent vertical deflection of the structure was recorded by using two linear variable differential transformers (LVDT). Two additional LVDTs were used for tracking the rotation at the end of the slab. In addition, measurements of the time dependent longitudinal deformation of the slab at midspan were also carried out with two strain gauges. The study has shown that the behaviour of slab under fire depends on the temperature of the prestressed strands, combined with the degradation of the modulus of elasticity of the heated concrete. Shear failure had no effect on the load bearing capacity of the slab.

Keywords: concrete, deformation, fire, hollow-core slab, LVDT, mechanical behaviour, prestressed steel, strain gauge, temperature measurements, vertical deflection

Ponašanje prednapetih šupljih betonskih ploča uslijed djelovanja požara – eksperimentalna analiza

Izvorni znanstveni članak

U radu je prikazan eksperiment u kojem je praćeno ponašanje prednapete šuplje betonske ploče pri djelovanju ISO krivulje razvoja požara. Analizirana šuplja ploča je dimenzija $1,2 \times 8,0$ m. U eksperimentu praćen je razvoj temperatura u nekoliko točaka: unutar ploče, u šupljinama i na površini ploče. Povećanje progiba ploče u vremenu praćeno je uz pomoć dva LVDT uređaja. Dva dodatna LVDT uređaja postavljena su na kraju ploče sa svrhom praćenja zaokreta ploče. Također, u eksperimentu je praćena promjena relativne uzdužne deformacije na sredini ploče uz pomoć dvije mjerne trakice. Rezultati eksperimenta pokazali su da nosivost i deformabilnost prednapete ploče uslijed djelovanja požara dominantno ovisi o razvijenoj temperaturi u prednapetim kablovima, te o degradaciji modula elastičnosti betona. Posmični lom nije imao utjecaja na ukupnu nosivost prednapete ploče.

Ključne riječi: beton, deformacija, požar, šuplje ploče, LVDT, mehaničko ponašanje, čelik za prednapinjanje, mjerne trakice, mjerenje temperature, progibi

1
Introduction

Prestressed hollow-core concrete flooring units represent a new trend in modern civil engineering building system. A hollow-core flooring system consists of several precast slab units, in combination with or without reinforced concrete topping. The benefits of using this type of flooring technology is: low weight of the floor structure, low on-site labour costs, relatively high strength of concrete ($60 \div 70$ MPa), and economical use of the concrete. The behaviour of prestressed hollow core slabs under normal temperatures has been described in modern engineering codes [1, 2] through simple calculation procedures of ultimate bending capacity of the slab. However, behaviour of hollow core slabs under fire temperatures is more complex. Different types of failure may occur during heating depending on restraining conditions at the end of the slab and depending on the length of the span.

The behaviour of prestressed hollow-core concrete slabs exposed to fire has been studied through a small number of experimental studies. In [3], three fire tests were conducted to determine the residual ultimate shear capacity of the slab with 3,3 m span and thickness of 26,5 cm. The three slabs were exposed to ISO standard fire for 60 minutes and to different load level. In study [4], three fire tests were conducted on slabs with 6,0 m span. In order to determine the ultimate load capacity of the slabs after being exposed to ISO fire, the thickness of the slabs varied from $18,5 \div 27$ cm. In study [5] focus of the research was on the influence of detailing and restraining conditions on the shear capacity of hollow core slabs

exposed to ISO fire. Four tests were done on two different types of slabs with 3,0 m span, with and without topping. In study [6], six slabs were exposed to ISO fire. Tests were performed on slabs ($5,2 \div 6,3$ m span) of different thickness ($20 \div 27$ cm), concrete type and topping. Conducted studies included temperature measurements at different positions on the slab (surface points, voids, prestressed strands, web of the slab). In order to record the mechanical response of the structure, vertical deflections of the slab were measured at midspan.

Studies have shown that different types of failure may occur in slabs during exposure to fire and that the load bearing capacity of the slabs depends on the length of the span (bending failure for slabs of 20 cm thickness and less, and shear failure in combination with the anchorage failure for thicker slabs). The reason for the occurrence of shear failure in some of the tests is a relatively small span of slabs on which tests were conducted. In addition, shear and anchorage failures have been observed in tests but never in real buildings because of the presence of axial restraints.

The purpose of this experiment is to study in more detail the behaviour of prestressed hollow-core slab exposed to standard (ISO) fire curve. This study is based on a hypothesis according to which slabs of realistic span ($\geq 8,0$ m), when exposed to fire, are more likely to reach their load bearing capacity because of bending failure than due to shear failure. Length of the span of the analysed slab is 8,0 m, which represents the realistic span for the chosen slab thickness of 20 cm. The study includes recording of the effects of the fire exposure on the slab by recording the strain, temperature and deflection changes in measuring points, which are representable for the entire

slab. Measurements of deformation, deflection and temperature parameters are necessary for the validation of a newly developed numerical model capable of simulating the thermo-mechanical behaviour of the slab during fire exposure.

2
Experimental study
2.1
Prior testing

In order to fully understand the behaviour of prestressed slab under fire exposure a thermo-mechanical numerical model was created to predict the temperature distribution over the slab, including the stress-strain distribution and vertical deformations. This model was used to estimate the load bearing capacity of the slab and the fire resistance time [7]. Additionally, the model was used to estimate the upper values of the deflection and rotation at the supports. In addition, a study of the behaviour of the concrete material under fire temperatures was done to obtain the basic input parameters for the numerical model. Concrete material study [8] included the determination of compressive and tensile strength, as well as secant and tangent modulus of elasticity of concrete at high temperatures (Fig. 1). Fig. 1 presents the measurement results of modulus of elasticity that were obtained on 9 different concrete samples. Analysed concrete mixture in study [8] is the same mixture that was used for casting of the tested slab. The study was done on cylindrical concrete specimens for a specified level of exposure to high temperatures. Two sets of samples were tested: hot samples (samples tested while heated to maximum temperature) and cold samples (samples tested after having been cooled to ambient temperature). In study [8] the concrete samples were heated up to 800 °C.

Prior to fire test, preloading of the slab was performed in order to test the sensor installations, acquire unknown constants of the mechanical system (composite modulus of elasticity [9] of the slab, lever arm and coefficient of load distribution). The slab was loaded with prescribed working load for 2 minutes, unloaded for 2 minutes and then loaded again for 8 minutes, as can be seen from Fig. 8.
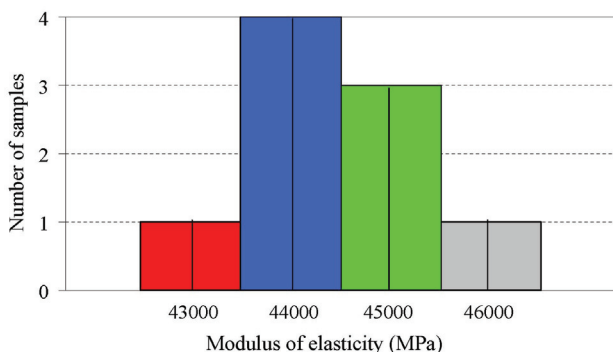

Figure 1 Histogram representing values of modulus of elasticity of concrete [8] at ambient temperatures

2.2
Test slab

Test slab is precast in manufacturing facility. Before the casting of the concrete, thermocouple wires were attached to prestressed strands in order to measure the temperature fluctuation in the prestressed strands. Disposition of the thermocouples is presented in Fig. 2. After the casting, the slab was left externally unloaded for a period of two years. Since internal forces due to prestressing were dominant, it is assumed that during time period of two years the concrete slab was exposed to conditions similar to the ones to which a real construction is normally exposed (creep of concrete due to prestressing, ageing of concrete and loss of prestressing force).

2.3
Steel frame structure for loading

Steel frame is utilized as a support for the hydraulic cylinders used to insert mechanical loading into the slab. Steel loading frame is a 3D steel structure with spatial dimensions 8280/3800/2400 mm. Loading frame is designed in a way that it does not have foundations, so that internal forces from loading of slab remain within the structure. The main vertical and horizontal elements are made of steel HE 320 A profiles, diagonals are made of HE 200 A profile (Figs. 3 ÷ 4). Steel elements of the frame were selected with a certain frame/slab bending stiffness ratio, so that the frame structure could have bending stiffness that is approximately 10 times higher than the stiffness of the tested slab. High bending stiffness ratio between the frame structure and the slab is necessary in order to prevent the bending of the steel frame during loading. Additional requirement on the bending stiffness ratio between the frame and the slab was made in order to exclude deformations of the steel frame from the conducted measurements. Since the displacement measuring equipment is attached to the frame structure, steel frame must have negligible deformations. Nonlinear static analysis of the steel frame showed that the maximum vertical deflection of the steel frame under static load did not exceed 0,13 mm. This value can be neglected when compared to the expected magnitude of the vertical deflections of the slab. Since the whole steel frame structure is comprised of steel elements connected with bolts, in order to prevent the bond slipping additional prestressing of bolts was done before the experiment.

2.4
Hydraulic cylinders

Hydraulic cylinders (H1) were used to insert mechanical load into the test slab. Test slab was exposed to constant work load in order to represent a realistic loading condition in the structure. Work load prescribed from manufacturer was 5,0 kN/m^2. To achieve similar load, taking into account the bending moments at midspan, test slab was loaded in thirds of span uniformly and transversely with 67,0 kN/m^2. To achieve this type of loading from cylinder, system of steel beams was used (Fig. 4). Weight of steel elements was added to the load and was equal to 2,5 kN. Pressure inside the cylinders was 60,0 bar, which is the equivalent of piston force in the cylinder equal to 17,5 kN. Pressure inside the cylinders was induced by using a hand pump and observed by using electronic pressure gage. In addition, the readout from pressure gage was digitalized in data acquisition system and recorded throughout the experiment.
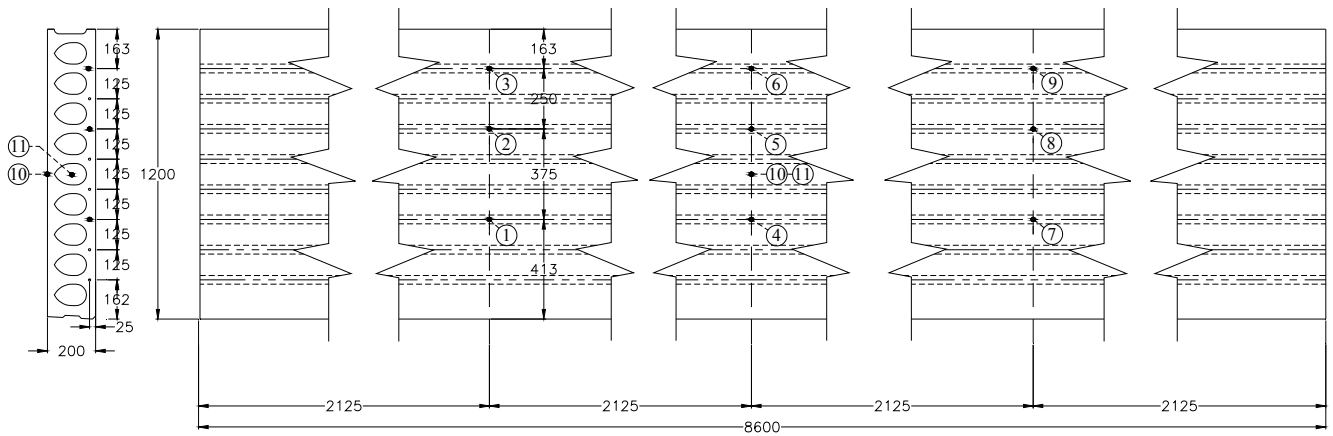
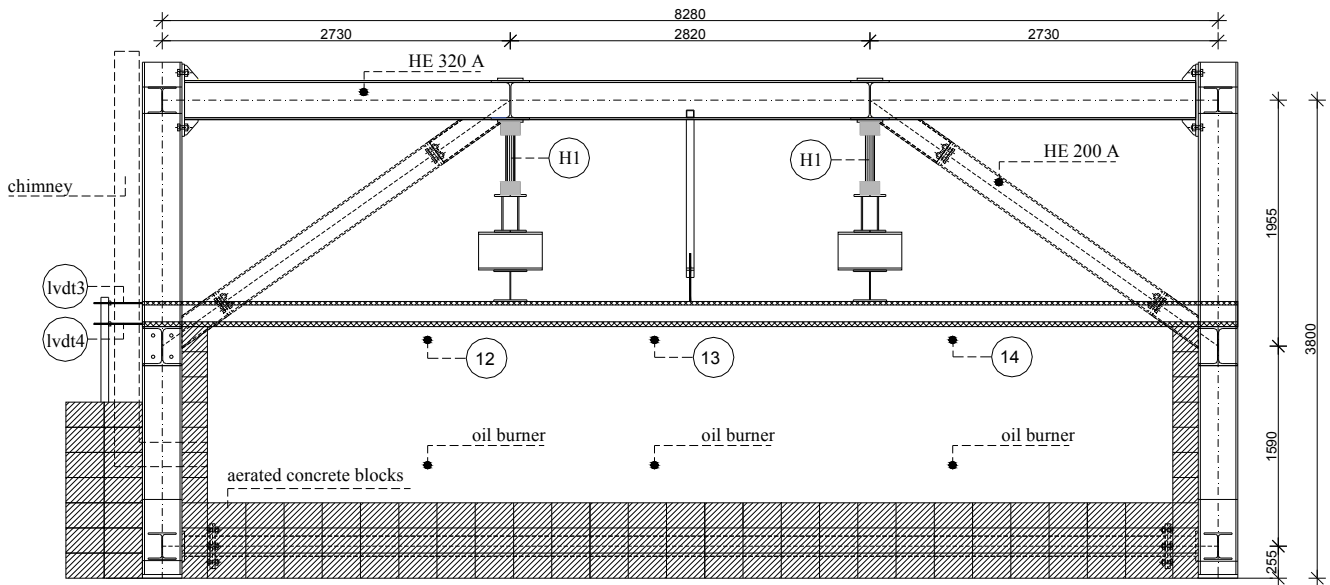**Figure 2** Disposition of the thermocouples on the slab

Figure 3 Steel frame structure for load insertion with the furnace – longitudinal view
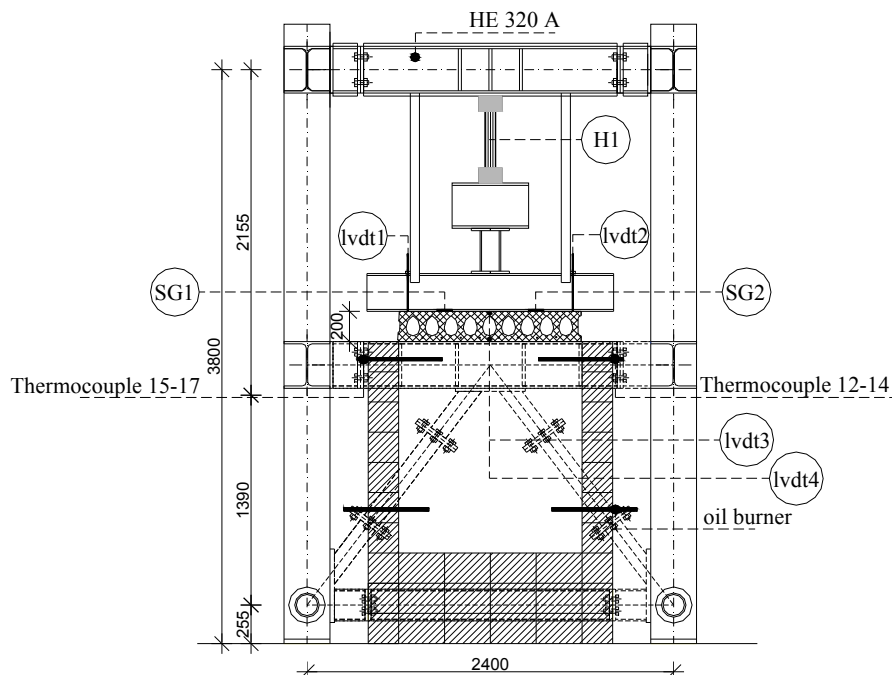

Figure 4 Steel frame structure for load insertion with the furnace – transverse view

Pressure transducer used in this experiment was SENSE STK131. Hydraulic cylinders used in the test were of A3060M0250P02 type manufactured by Hydromat. Cylinder bore was 63 mm and piston stroke 250 mm.
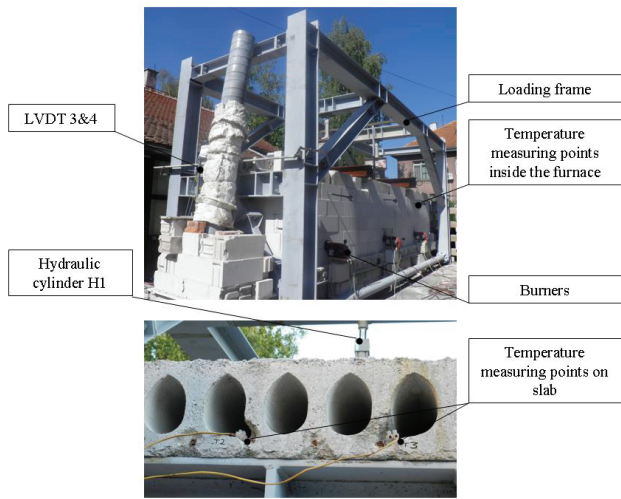
Figure 5 Test setup

2.5
Fire load setup and measurements

In order to expose test slab to fire temperatures, furnace was placed at the bottom side of the slab (Fig. 5). The furnace was built using lightweight, aerated concrete bricks with low values of thermal conductivity (0,13 W/(m·K)). In addition, interior walls of the furnace were covered with light thermal insulation made of ceramic fibres.

The purpose of the closed and isolated furnace was to hold uniform temperature inside the furnace, and to prevent transmission of heat to any other object other than test slab. The possible transmission of heat would have damaged the equipment and introduced errors in measurements (e.g. fire temperatures in contact with steel frame would have compromised the accuracy of force measurement). To control this, temperature of the steel frame was measured during the experiment. In addition, the gaps between the test slab and the steel frame were filled with soft thermal insulator. The dimensions of the furnace were 7,6/1,4/1,2 m and the thickness of the walls was 20,0 cm.

Openings through the walls were made on lateral sides of the furnace for insertion of oil burners. Burners used in this experiment were controlled by a computer unit. Six burners were used to obtain fire temperatures underneath the slab.

Figure 6 Results of temperature measurements inside the furnace

Burners used for applying fire load were manufactured by Bentone, type B30A. Burners were

fuelled by light oil. The average power delivered from burners to the furnace in order to increase its temperature was 97 kW. Burner control system was used to achieve ISO fire curve [10]. Six thermocouples (thermocouples 12 ÷ 17 from Fig. 3) were used to control the temperature increase in the burners. They were positioned approximately 1,0 m above the burners and were protected from the direct exposure to radiation of the flames. Type K (NiCr-Ni) thermocouples with 3 mm thick wires were used. Fig. 6 presents a comparison between the ISO curve and the obtained temperatures in the furnace.

2.6
Temperature measurement of the slab

Temperature was measured on the upper surface of concrete slab, on prestressing strands and in the middle void. Sensors that measured temperature of strands had been mounted before the concrete was cast. A total of 9 thermocouples were attached to prestressing strands (thermocouples T1-9 from Fig. 2). Additional thermocouples were placed in hollow area of the slab (T9) and on the top surface near strain gauges and LVDT devices (T10). Thermocouples used for measuring the temperature of the slab were of type K with 0,5 mm thick wire. Temperature sensor data was conditioned using National Instruments modules for thermocouples and digitalized using NI DAQ (data acquisition). Fig. 7 presents the results of the measured temperatures in the slab and the ISO fire curve.
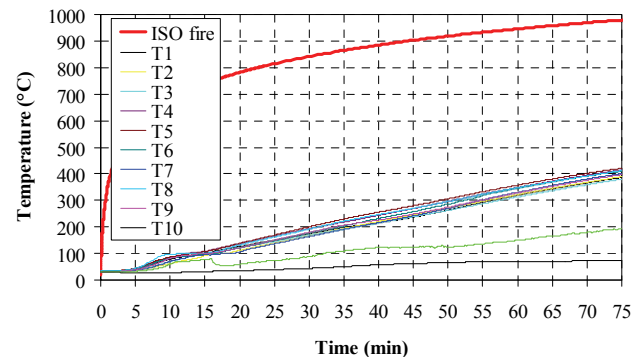

Figure 7 Results of temperature measurements in the slab

2.7
Measurement of mechanical quantities

Mechanical quantities measured and recorded in the test were displacements at midspan, longitudinal strains on the upper side of the slab at midspan and the rotation of test slab at the support.

Displacements were measured using linear variable differential transformer [11]. LVDT devices used in this experiment were HB 500 mm stroke plunger type with WA electronics conditioned LVDT. Transducers were mounted vertically at midspan, transversely in thirds of the slab's width (Figs. 3 ÷ 4). Verticality of transducer was achieved by using level. The maximum deflection that was measured from vertical position was 0,157°. Signal was electronically conditioned inside WA electronics and fed to data acquisition card.
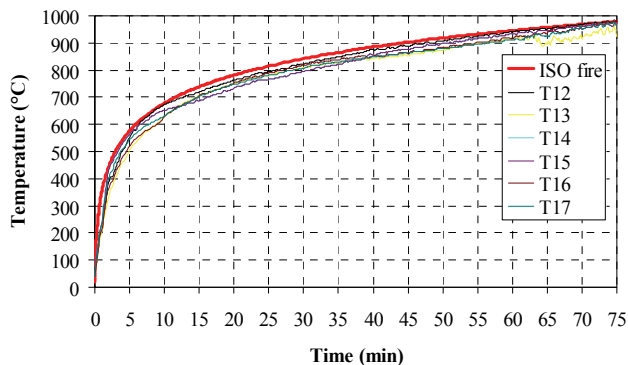
Deformations were measured using two strain gauges [12]. Strain gauges used for this experiment were HBM 1-LY41-100/120. This type of strain gauge had a temperature compensation for steel and concrete. Strain gauges were installed using adhesive for concrete prescribed by manufacturer. Sensors were installed 3 days before measurements to ensure curing of adhesive. The slab was unloaded at installation time and temperature of top surface of the slab was 26,4 °C. Strain gauges were wired in quarter bridge, with temperature compensation using passive unstrained gauge on the same arm of bridge. Excitation voltage of bridge was recorded during experiment and it is on an average 5,36 V with tolerance of 0,5 %. Main source of energy supply used in the test was regulated laboratory supply. Signal from strain gauges was connected to instrumentation amplifier with gain of 1000 to data acquisition input. Range of output from amplifier is 2,8 V for strain gauge SG1 and 3,1 V for strain gauge SG2. Cables used for connecting equipment were shielded and strain gauges were grounded near measurement point. Temperature sensor was placed near strain gauges to monitor surface temperature. Because of warm weather and insolation during testing surface minimum temperature was 27,7 °C and maximum surface temperature of the slab after the experiment was 75 °C.

Rotation of the slab at the support was measured by using two parallel horizontal LVDTs. The vertical distance between the two LVDTs was 18 cm. Measurements of the horizontal displacements were used to reconstruct the rotation of the slab at the support. Rotation was calculated from measured displacements using formula:

$$\alpha = \arctan\left(\frac{L_1 - L_2}{d}\right), \tag{1}$$

where L_1 and L_2 are displacements from LVDT3 and LVDT4 respectively, while d is distance between the two LVDTs. Custom grips were built for this measurement in order to ensure constant distance (d) between the LVDTs.

2.8
Signal conditioning

For data acquisition two NI USB 6255 were used. First DAQ was used for acquisition of measurements of displacement, rotation and pressure. Second DAQ was used for measurements of longitudinal strain. Because of large time constant of measured system, signals were sampled at frequency of 1 Hz. All inputs were arranged as differential input to achieve better signal to noise ratio in noisy environment. Software for data acquisition was created in MATLAB [13]. Acquisition was continuous. Signals were filtered using LOWESS [14] (locally weighted scatter plot smoothing) to first order polynomial with span of 10 points to remove environmental noise.

Strains ε were calculated using output voltage from amplifier, surface temperature and excitation voltage according to Eq. (2). Nonlinearities from calibrations were taken into account in conditioning of signals [9].

$$\varepsilon = \frac{(1+t)\left[2V_{\text{OUT}}(R_g^a + R_g^p) - V_{\text{EX}}(R_g^a - R_g^p)\right]}{kR_g^a(V_{\text{EX}} - 2V_{\text{OUT}})g}. \tag{2}$$

R_g^a – resistance of unstrained active strain gauge; R_g^p – resistance of unstrained passive strain gauge; V_{EX} – voltage of bridge excitation; k – gauge coefficient; t – temperature compensation coefficient; g – gain from amplifier.

2.9
Theoretical relationship between measured mechanical quantities

In apparently simple mechanical system as a simply supported beam theoretical link between displacements, strains and rotation on supports is known. Using Eq. (3) ÷ (5) relations between displacements, rotations, strains and external load were calculated. These relations are valid if stresses in the material are low considering the strength of material: 15 MPa is the upper value of stress in the concrete slab according to thermo-mechanical model predictions, while the compressive strength of concrete at ambient temperature is 65 MPa [7]. For ambient temperatures calculated values correlate very well with the measured values. During fire exposure, more complicated relations are required. This test setup is an important part of exploring these relations. Concomitant measurements of the mechanical quantities were used to determine unknown constants of the mechanical system and to check data validity. Unknown constants for this test were: composite modulus of elasticity of the slab at ambient temperature (combined steel and concrete), ratio of two forces used as an external load on slab and lever arm of internal forces in the slab at ambient temperature. To calculate the unknown parameters preloading sequence on the slab as stated in chapter 2.1 was performed. For the analysed mechanical system relation between deflection and load [15] is given in (3):

$$f(L/2) = \frac{F \cdot a_1}{48 \cdot E_{c,20} \cdot I_y} \cdot \left(3 \cdot L^2 - 4 \cdot a_1^2\right) + $$
$$+ \frac{k_H \cdot F \cdot a_2}{48 \cdot E_{c,20} \cdot I_y} \cdot \left(3 \cdot L^2 - 4 \cdot a_2^2\right), \tag{3}$$

$f(L/2)$ – midspan deflection of the slab; F – applied force in the cylinder; a_1 and a_2 – distance between the edge of the slab and the point to where the force is applied; k_H – ratio of applied forces; $E_{c,20}$ – composite modulus of elasticity at ambient temperature; I_y – moment of inertia of test slab.

Relation between rotation of slab at the support and the external load is given in (4):

$$\varphi_A = \frac{F \cdot a_1}{6 \cdot L \cdot E_{c,20} \cdot I_y} \cdot \left(2 \cdot L^2 - 3 \cdot L \cdot a_1 + a_1^2\right) + $$
$$+ \frac{k_H \cdot F \cdot a_2}{6 \cdot L \cdot E_{c,20} \cdot I_y} \cdot \left(L^2 + a_2^2\right), \tag{4}$$

φ_A - rotation of the slab at support.

Relation between longitudinal strain at midspan and the applied external load is given in (5):

$$\varepsilon_{xx} = z \cdot \frac{F \cdot a_1 + k_H \cdot F \cdot a_2}{2 \cdot E_{c,20} \cdot I_y}, \tag{5}$$

ε_{xx} – strain in longitudinal direction; z – lever arm between the compressive and tension force in the slab. Unknown values were calculated by using minimization of error function where error is defined as a sum of squared relative difference between calculated values according to Eq. (3) ÷ (5) and corresponding measured

values. Approximate value of composite modulus of elasticity at ambient temperature $E_{c,20}$=44,1 GPa was taken from study [8].The value of composite modulus at ambient temperature was determined as a mean value of results presented in Fig. 1 (9 samples). Calculated values of constants were: $E_{c,20}$ = 0,9464×44,1 GPa, z = 0,09 m, k_H = 1,069. Moment of inertia used in the calculation was I_y =70 398 cm^4. Results of the concomitant measurements of mechanical quantities and corresponding calculated mechanical quantities are presented in Fig. 8. At the bottom of Fig. 8, load scheme of the analysed mechanical system is shown.
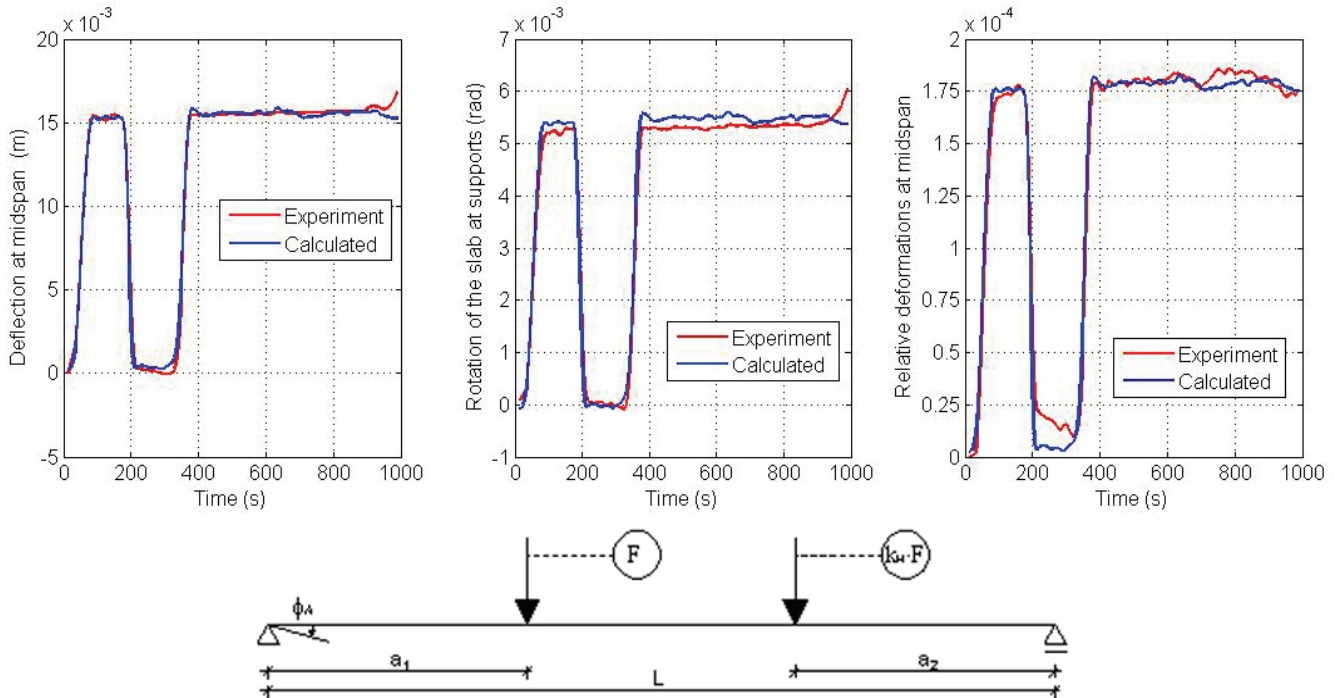

Figure 8 Comparison of results between measured and calculated values of deflection, rotation and longitudinal deformation

Table 1 Error assessment for displacement and rotation sensors

Transducer	Relative error (%)				Overall error (%)
	Error due to positioning of transducer	Errors due to nonlinearity of sensor	Error due to environmental effects	Error due to quantization (16 bit ADC)	
L_3 – 100 mm stroke	0,27	0,09	0,22	0,00076	0,581
L_4 – 100 mm stroke	0,27	0,11	0,18	0,00076	0,561
L_1 – 500 mm stroke	0,27	0,07	0,16	0,00076	0,501
L_2 – 500 mm stroke	0,27	0,11	0,40	0,00076	0,781

2.10
Analysis of measurement errors
2.10.1
Measurement of displacements and rotation of slab at the supports

Errors that were taken into account [16]: errors in positioning sensors, errors due to nonlinearity of sensor, errors introduced from conditioning electronics, errors due to environmental effects and errors of analog to digital converter (Tab. 1).

2.10.2
Pressure measurement

Errors in pressure measurement were errors deriving from the lack of accuracy of transducer, thermal effect on sensor, environmental effects error, quantization error from analog to digital converter and shunt error in conversion from current output to voltage output. Accuracy of transducer was 0,5 % for range 0 ÷ 300 bar. Thermal effect on transducer was 0,02 % for full scale /

K. Error from shunt resistor was 0,1 %. Overall relative error was 1,49 %.

2.10.3
Strain measurements

Absolute error of strain gage measurement was calculated using Eq. (6):

$$\Delta\varepsilon^2 = \left|\frac{\partial\varepsilon}{\partial t_{komp}}\right|^2 \Delta t_{komp}^2 + \left|\frac{\partial\varepsilon}{\partial V_{OUT}}\right|^2 \Delta V_{OUT}^2 + \left|\frac{\partial\varepsilon}{\partial V_{EX}}\right|^2 \Delta V_{EX}^2 +$$
$$+ \left|\frac{\partial\varepsilon}{\partial R_g^a}\right|^2 (\Delta R_g^a)^2 + \left|\frac{\partial\varepsilon}{\partial R_g^p}\right|^2 (\Delta R_g^p)^2 + \left|\frac{\partial\varepsilon}{\partial k}\right|^2 \Delta k^2, \quad (6)$$

where Δ symbol represents absolute error of the quantity standing next to. According to strain gauge datasheet and measurements taken prior to installation of sensors, values are:

$R_g^a = 120,21\,\Omega$

$\Delta R_g^a = 0,01\,\Omega$

$R_g^p = 120,21\,\Omega$

$\Delta R_g^p = 0,01\,\Omega$

$t_{komp} = 0$

$\Delta t_{komp} = 10\times10^{-6}\,°C$

$V_{EX} = 5\,V$

$\Delta V_{EX} = 0,001\,V$

$k = 2,07$

$\Delta k = 0,01\cdot 2,07 = 0,0207.$

Substituting known values into Eq. (6), the absolute error of strain gauge measurements of $5,91\times10^{-5}$ is obtained.

2.10.4
Temperature measurements

Transducer error for temperature measurement using K type thermocouples was ±2,2 °C for temperatures over 200 °C. Error of system for measuring temperature was 0,564 °C for full temperature scale (30 ÷ 1000 °C). Overall error was 2,764 °C for full temperature scale.

2.11
Assessment of composite modulus of elasticity of the slab at high temperatures

Composite modulus was assessed under the assumption that the distribution of temperature in the cross section of the slab is nonlinear. Total measured deflection consists of two components:

$$f_{TOTAL} = f_{FORCE} + f_{TEMP}, \quad (7)$$

where: f_{FORCE} − deflection due to external load coupled with the effect of steel and concrete softening at high temperatures, f_{TEMP} − deflection due to temperature difference between upper and lower surface of the slab and f_{TOTAL}− total measured deflection.

Deflection f_{FORCE} from Eq. (7) was used to calculate composite modulus of elasticity of the slab $E_{c,20}$, by extracting the modulus from Eq. (3). For mechanical system of simply supported slab, the deflection from temperature difference is given by:

$$f_{TEMP} = \frac{\left[\varepsilon\cdot(T_{lower}) - \varepsilon\cdot(T_{upper})\right]\cdot L^2}{8\cdot h}, \quad (8)$$

where: h − height of the slab, T_{upper} − temperature from the upper zone of the slab, T_{lower} − temperature from the lower zone of the slab. Expression for thermal strain $\varepsilon(T)$ of concrete was taken from reference [17].

Temperatures T_{upper} and T_{lower} were calculated by using measured temperatures:

$$T_{upper} = (T_{strand} - T_{surface})\cdot 0,8133 + T_{surface},$$
$$T_{lower} = (T_{strand} - T_{surface})\cdot 0,03413 + T_{surface}, \quad (9)$$

where T_{strand} − measured mean strand temperature, $T_{surface}$ − measured surface temperature. Temperatures T_{upper} and T_{lower} are presented in Fig. 9.
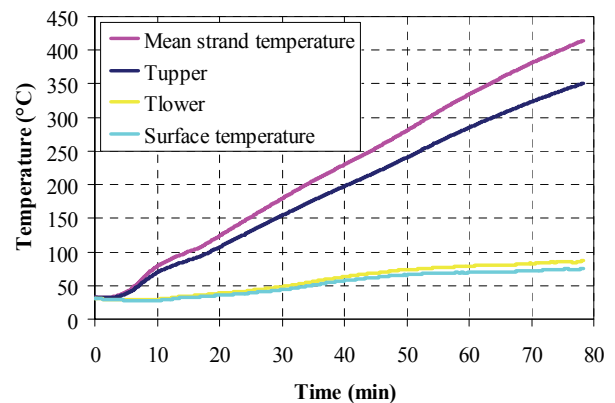

Figure 9 Temperatures used for calculating modulus $E_{c,20}$ plotted in Fig. 13.

3
Test results

Fig. 10 presents the increase of the vertical deformation of the slab with respect to time. It can be seen that vertical deformations measured by LVDT1 and LVDT2 are almost identical.
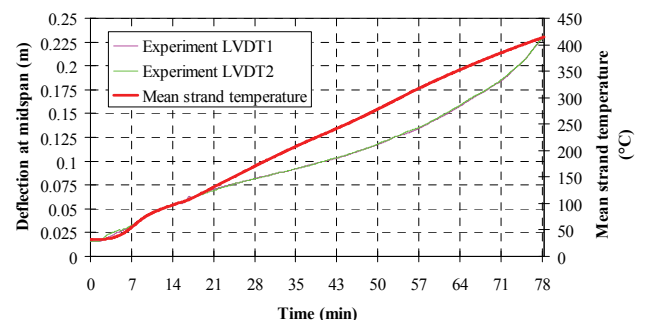

Figure 10 Deflection of slab at midspan with respect to time and measured mean strand temperature

Fig. 11 presents the increase of the rotation of the slab at supports with respect to time. Similar trend of change for deflection and rotation can be observed from Figs. 10 and 11.
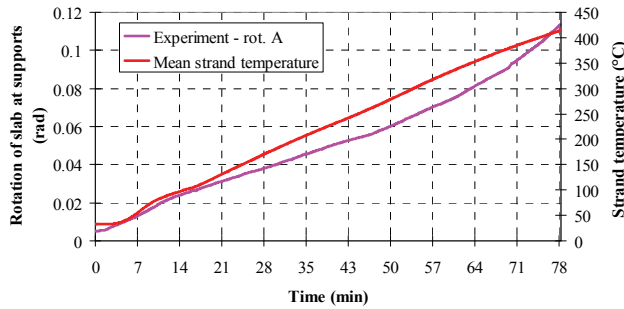

Figure 11 Rotation of the slab at the support with respect to time

Fig. 12 presents the changes in the longitudinal strain at midspan with respect to time. Blue line indicates the approximate time when a large longitudinal crack develops over the slab.
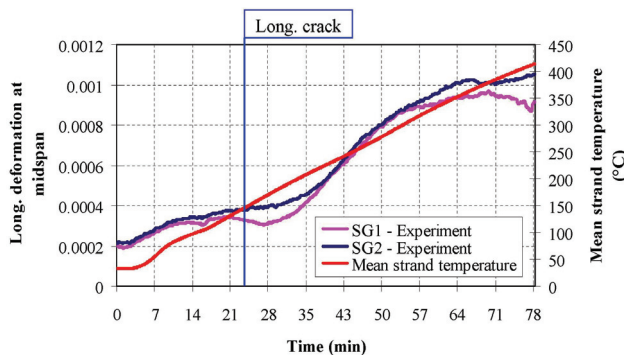

Figure 12 Longitudinal deformation at midspan with respect to time

Fig. 13 presents the calculated composite modulus of elasticity of the slab (combined concrete and prestressed strands) with respect to time.
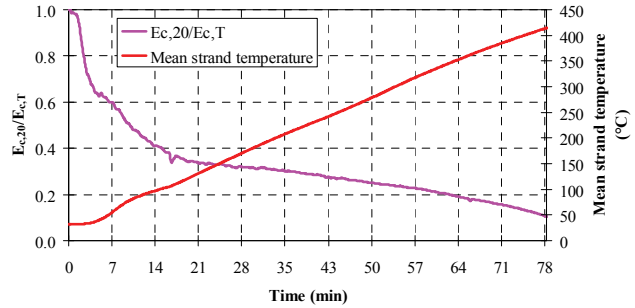

Figure 13 Reduction of the composite modulus of elasticity of the slab at high temperatures with respect to time

Analytical formulations were derived by using curve fitting techniques to fit measured mechanical quantities in dependence on mean strand temperatures. Fig. 14 shows both measured and fitted data and their respective residues. All of the experimental data was fitted to polynomial form. Method for fitting data was least square robust fitting with bisquare weights. Fitting of the measured data has yielded Eq. (10) ÷ (12): For mean deflection at midspan with respect to temperature Eq. (10) was derived, for rotation of the slab at supports Eq. (11) was derived and for mean deformations at midspan Eq. (12) was derived.

$$d_f(t) = 6{,}321 \times 10^{-9} \cdot t^3 - 3{,}751 \times 10^{-6} \cdot t^2 + \\ + 1{,}032 \times 10^{-3} \cdot t - 1{,}631 \times 10^{-2} \quad (m) \tag{10}$$

$$s_{2f}(t) = -1{,}278 \times 10^{-5} \cdot t^6 + 4{,}092 \times 10^{-5} \cdot t^5 - \\ - 7{,}817 \times 10^{-5} \cdot t^4 - 2{,}068 \times 10^{-4} \cdot t^3 + \\ 1{,}498 \times 10^{-4} \cdot t^2 + 4{,}749 \times 10^{-4} \cdot t + 5{,}607 \times 10^{-4} \quad (rad) \tag{11}$$

$$r_f(t) = 2{,}276 \times 10^{-9} \cdot t^3 - 1{,}302 \times 10^{-6} \cdot t^2 + \\ + 4{,}297 \times 10^{-4} \cdot t - 7{,}908 \times 10^{-3} \quad (m/m) \tag{12}$$
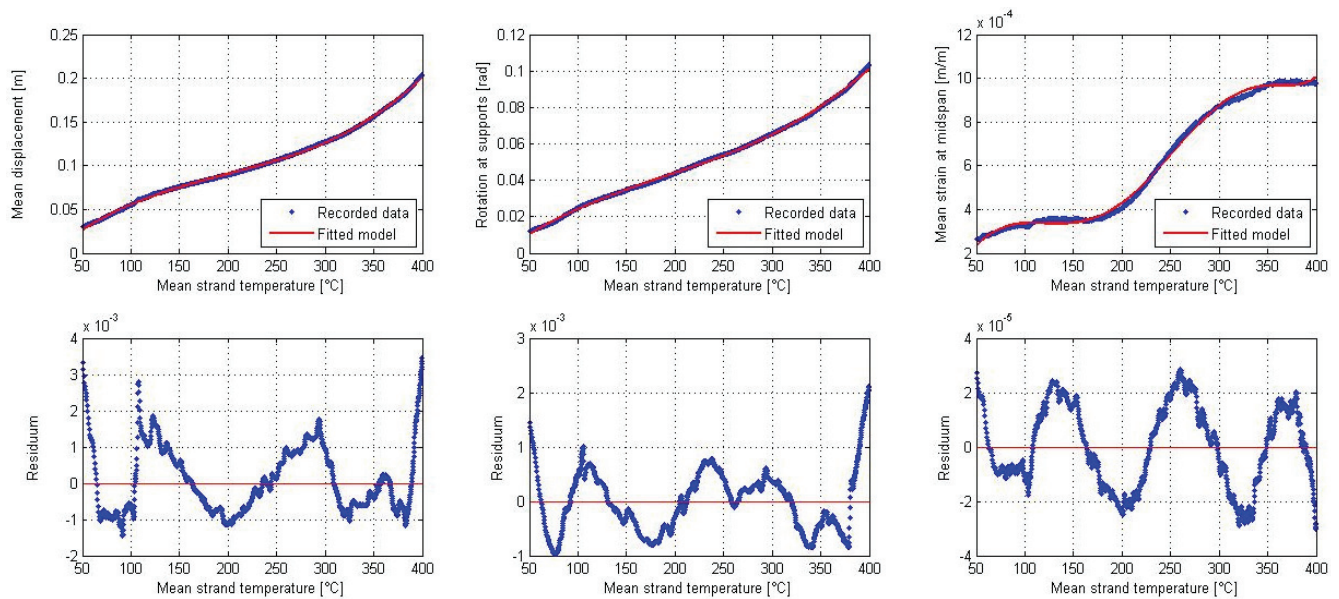
where *t* represents mean strand temperature in °C.

Figure 14 Comparison of measured and fitted data for mean displacement, rotation at supports and mean strains in temperature range 50 ÷ 400 °C

4
Discussion of results

The test was terminated when the deflection of the slab reached the value of approximately $L/30$, where L is the length of the heated span of the slab. After reaching that deflection limit, fire test is usually stopped because it is generally considered that failure of slab occurs afterwards. Results from Fig. 6 show that approximately uniform temperature in the furnace has been achieved, with the temperature inside the furnace being close to ISO curve. It can be seen from Fig. 7 that uniform heating of the slab has been achieved and that temperature difference between the 9 measuring points is very low.

During the experiment, a large longitudinal crack along the slab developed between the 15th and 25th minute (Fig. 15). Possible cause of the longitudinal crack is the fact that there are no transverse steel reinforcements in the slab to prevent the thermal expansion of concrete. Figs. $10 \div 11$ show that longitudinal cracking did not affect the vertical deformations and the rotation of the slab at the supports, which points out to the fact that longitudinal crack has no effect on reduction of bending stiffness of the slab. However, strain gauges have registered the cracking between the 15th and 25th minute, which can be seen in Fig. 12. In that time period, stress and strain redistribution at midspan occurs because of cracking. In later time period, when the redistribution of stresses is finished, strain change in both of the strain gauges is similar. This also contributes to the fact that large longitudinal cracking did not affect the bending resistance of the slab at high temperatures.

Figure 15 Test slab with a large longitudinal crack at the end of experiment

Fig. 12 also shows a large increase in the values of strain when compared to strain values before heating of the slab (approximately five times higher). Fig. 13 shows a large reduction of the composite modulus of elasticity of the slab during the first 30 minutes. Large reduction occurs because of the existence of additional deformations in the concrete when exposed to high temperatures (transient and creep strains) which considerably affect the vertical deformations of the slab (Fig. 12). In addition, modulus of elasticity of the prestressed strands is also reduced with respect to temperature of the strands. Reduction of the modulus of strands is approximately 50 % at the temperature of 400 °C [5], which also contributes to the degradation of the composite modulus of elasticity of the slab.

In addition to a developed longitudinal crack during testing, shear cracks at the supports have been revealed after the test (Fig. 16). Shear cracks appear not to affect the vertical deformations of the slab, as can be seen from Fig. 10 because there are no sudden vertical deflections in short time periods. Thus, the loss of shear resistance of the slab is not critical for the analysed slab. Temperature increase in the slab has greater influence on bending resistance of the slab. The results of this study can be compared only with the results of study [6] due to similar testing methodology (loading and heating conditions). However, all of the slabs that were tested in study [6] exhibited shear failure in combination with the anchorage failure. Occurrence of large longitudinal cracks on slabs was also observed in study [6].

Figure 16 Shear cracks in the vicinity of supports

After having observed all the values measured in the experiment and having in mind the characteristics of the mechanical system, it can be concluded that the measurement has been done in a sufficient number of points in order to find out the unknown parameters of the mechanical characteristics of the slab exposed to high temperatures. Having observed temperatures inside the furnace (with maximum deviation of 50 °C in the measuring points) as well as inside the slab (with maximum deviation of 40 °C in the measuring points), the uniformity of temperature can be confirmed, which is one of the main postulates of the experiment.

5
Conclusions

- Large longitudinal crack along the slab develops between the 15th and 25th minute, due to the transverse thermal elongation of the slab, because there are no transverse reinforcements to counteract the developed cracks;
- Shear cracks develop at the end of the slab near the supports, however, they have not affected the overall deformability, or the load bearing capacity of the slab;

- Vertical deformability of the slab depends solely on the additional deformations that occur in concrete during heating and on values of temperature in the prestressed strands;
- Study has shown that relevant parameters have been measured in a suitable number of points on the slab (temperature, deflection and strain increase);
- Test results have confirmed that when using realistic span for slab testing, shear failure has no influence on the load bearing capacity of the slab;
- Further research will be focused on additional testing of slabs with greater thickness in order to confirm that bending failure is the dominant failure mode of the slabs which are tested on slabs of realistic span.

Acknowledgement

6
References

[1] EN 1992-1-1:2004, Eurocode 2 - Design of Concrete structures - Part 1-1: General Rules and Rules for Buildings, European Committee for Standardization, Brussels, 2004.

[2] EN 1168:2005+A1:2008, Precast Concrete Products – Hollow Core Slabs, European Committee for Standardization, Brussels, 2008.

[3] Betonelement-Foreningen. Hollow Core Slabs and Fire – Documentation on Shear Capacity, Birch&Krogboe A/S, Copenhagen, 2005.

[4] Andersen, N. E.; Lauridsen, D. H. Technical Report X 52650 Part 2 – Hollow Core Concrete Slabs, Danish Institute of Fire Technology, Hvidovre, 1999.

[5] Dotrepe, J. C.; Fransen, J. M. Precast Hollow Core Slabs in Fire: Numerical Simulations and Experimental Tests, The Third International Workshop Structures in Fire, Ottawa, Canada, paper S5-1, 2004.

[6] Wozniak, G.; Lukomski, M.; Borowy, A. The Determination of the Fire Resistance of Prestressed Hollow Core Concrete Slabs, Proceedings of the International Conference Concrete for Fire Engineering, Dundee, Scotland, 2008, pp. 291-302.

[7] Torić, N.; Harapin, A.; Boko, I. Numerical model for determining fire behaviour of structures. // Građevinar, 64, 1(2012), pp. 1-13.

[8] Torić, N.; Jelčić-Rukavina, M.; Bjegović, D.; Peroš, B. Short term reduction of mechanical properties of high strength concrete after cooling to ambient temperature, 2nd International RILEM workshop on concrete spalling due to fire exposure, 5-7 October 2011, Delft Netherlands, 2011, pp. 173-180.

[9] Ferrito, J. M. An Evaluation of the Accuracy of Material Model Representation of Reinforced Concrete. // Experimental Techniques, 5, (1981), pp. 10-18.

[10] ISO 834: 1975 Fire-resistance tests – elements of building construction, International Organization for Standardization, 1975.

[11] Regtien, P. P. L. Measurement Science for Engineering, Kogan Page Science, London, 2004.

[12] Hoffman, K. An Introduction to Measurement using Strain Gages, Hottinger Baldwin Messetechnik GmbH, Darmstad, 1989.

[13] MATLAB 7 Users Guide, Matworks, 2010.

[14] Pavese, F.; Forbes, A. B. Data Modeling for Metrology and Testing in Measurement Science, Birkhäuser, Boston, 2009.

[15] Šimić, V. Resistance of materials 1, 2nd ed., Školska knjiga, Zagreb, 2002. (on Croatian)

[16] Figiola, R. S.; Beasley, D. E. Mechanical Measurements, 5th ed., John Wiley & Sons Inc., Hoboken, 2011.

[17] EN 1992-1-2:2004, Eurocode 2 - Design of Concrete Structures - Part 1-2: General Rules - Structural Fire Design, European Committee for Standardization, Brussels, 2004.

Authors' adresses

Neno Torić
University of Split
Faculty of Civil Engineering, Architecture and Geodesy
Matice Hrvatske 15, Split, Croatia
E-mail: neno.toric@gradst.hr

Vladimir Divić
University of Split
Faculty of Civil Engineering, Architecture and Geodesy
Matice Hrvatske 15, Split, Croatia
E-mail: vladimir.divic@gradst.hr

Ivica Boko, Ph.D.
University of Split
Faculty of Civil Engineering, Architecture and Geodesy
Matice Hrvatske 15, Split, Croatia
E-mail: ivica.boko@gradst.hr